Proceedings of the Southern Power Electronics Conference (SPEC 2016), Auckland, New Zealand, December 5-8, 2016

Eddy-Current-Based Contactless Speed Sensing of Conductive Surfaces

A. Tüysüz,
M. Flankl,
J. W. Kolar,
A. Mütze

Eddy-Current-Based Contactless Speed Sensing of Conductive Surfaces

Arda Tüysüz, Michael Flankl and Johann W. Kolar
Power Electronic Systems Laboratory
ETH Zurich
Zurich, Switzerland
Email: {tuysuz, flankl, kolar}@lem.ee.ethz.ch

Annette Mütze
Electric Drives and Machines Institute
Graz University of Technology
Graz, Austria
Email: muetze@tugraz.at

***Abstract*—Contactless speed sensors are used in a broad area of applications in various industries such as machining, assembly lines and transportation. Commonly used technologies are based on optics (e.g. cameras, encoders), or electromagnetic effects (e.g. variable reluctance sensors, Hall sensors). However, these sensors require a non-uniform property of the moving target that can be detected. For example, variable reluctance sensors rely on the variation of the air gap, and Hall sensors require a magnetic field whose spatial distribution is dependent on the position of the mover. A clear disadvantage of all these systems is the fact that they require modifications on the target's geometry and/or magnetic properties, since they cannot measure the speed of a smooth body/surface. Moreover, some of them are sensitive to environmental conditions; e.g. dirt in case of optical encoders and high temperature in case of permanent magnets can render these systems ineffective. Therefore, an eddy-current-based contactless speed sensor is developed in this work for measuring the speed of smooth, electrically conductive surfaces in harsh operating conditions. An injection coil is used to induce eddy currents in the mover whose speed is to be detected, and two differentially wound pick-up coils are used to detect the speed-dependent deformation of the eddy-current field. Two-dimensional finite-element method (2-D FEM) is used for modeling the system and optimizing the sensor geometry as well as the injection frequency. Measurements taken from a prototype verify the validity of the design procedure and the analyzed speed-sensing concept.**

I. Introduction

Measuring the speed of a moving (i.e. rotating or translating) body is essential for realizing a closed-loop control in a broad range of industries such as machining, assembly lines and transportation. Direct contact of the speed sensor with the moving body's surface is either prevented by the operating context, or undesirable due to reliability concerns in numerous applications. Therefore, several types of contactless speed sensors are used such as variable reluctance sensors, Hall sensors or encoders. However, these sensors require a non-uniform property of the moving target that can be detected, e.g., variable reluctance sensors rely on the spatial variance of the magnetic permeance, Hall sensors of the magnetic field distribution and encoders of the optical properties. Hence, these sensors cannot be used for measuring the speed of smooth surfaces. More advanced speed sensing methods such as using image processing (as done in optical computer mice) can measure the speed of rather smooth surfaces, but they are not considered here since they cannot operate reliably in harsh environments.

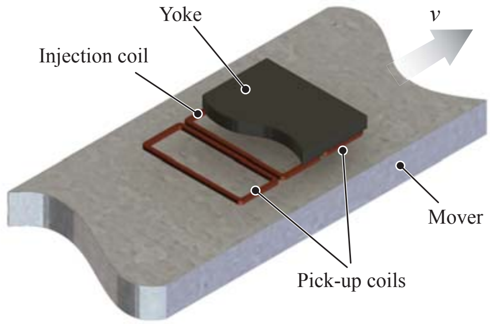

Fig. 1: Construction of the analyzed speed sensor comprising a magnetic yoke, an injection coil and two pick-up coils. A cut-away view is shown in the image to visualize the coils. The yoke of the actual system covers all three coils.

An interesting contactless speed sensing method is presented in [1], where a U-shaped inductor is used to place a magnetic mark on a moving steel band, whose speed is estimated based on the time delay between the detections of the magnetic mark by two magnetic field sensors placed at different downstream locations. However, this method cannot be used for estimating the speed of non-magnetic metals such as aluminum. The magnetic marker is eliminated in [2], where two eddy-current sensors are used for detecting the inhomogenities in the rail above which they are moving. The speed is estimated via the cross-correlation of the two sensor output signals.

In this work, a single, differentially wound eddy-current sensor is employed for measuring the speed of an electrically conductive surface, which does not need to be made of a magnetic material or feature any inhomogenities. A sketch of a possible sensor arrangement is shown in **Fig. 1**. When an AC current is flowing in the injection coil and the mover is in motion ($v \neq 0$), there is a slight difference in the induced voltages in the pick-up coils, which is measured and processed for estimating the speed. Similar speed sensor arrangements have been presented in literature (e.g. [3]), but these works

978-1-5090-1546-7/16/$31.00 ©2016 IEEE

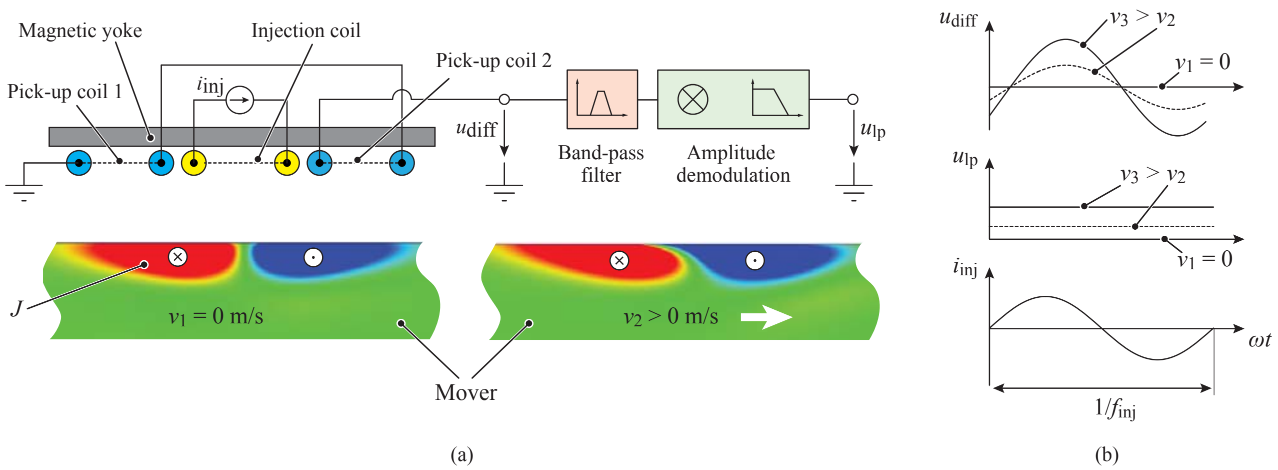

Fig. 2: Operating principle of the speed sensor used in this work. (a) An injection coil is used for generating the eddy currents (J) in the mover. The current distribution is depicted for two different speeds: v_1 = 0 m/s, and $v_2 > 0$ m/s. Since the current distribution is skewed due to the speed of the mover, the reaction field induces different voltages in the two differentially wound pick-up coils. (b) The difference of the induced voltages is measured, filtered and amplitude demodulated. The resulting output voltage u_{lp} is proportional to speed.

have not considered a magnetic yoke. In this work, the sensor topology is further improved by the addition of a magnetic yoke.

The principle of operation is detailed further in **Sec. II**. **Sec. III** describes the design aspects (i.e. goals, constraints and degrees of freedom of optimization) as well as the electromagnetic modeling method. Effects of different degrees of freedom on the sensor performance are also analyzed. The hardware prototype and the test setup are introduced in **Sec. IV**, and the results of the earlier analysis are compared to the measurements. Finally, **Sec. V** recaps the important findings and concludes the paper.

II. Principle of Operation

An AC current injected in the injection coil excites eddy currents in the electrically conductive mover. The eddy-current distribution in the mover depends on several factors such as the amplitude $\hat{i}_{inj}$ and the frequency f_{inj} of the injected current i_{inj}, the air gap length g, the material properties of the mover as well as its speed v. The eddy-current distribution is symmetric at standstill, but a non-zero speed results in a skewing of the eddy-current distribution, as shown in **Fig. 2(a)**. This skewing results in a slight difference of the magnetic flux density on the two sides of the injection coil. This speed-dependent effect is detected via the two pick-up coils arranged symmetrically on both sides of the injection coil, which are wound in opposite directions, such that the difference of induced voltages (u_{diff}) can be obtained with a single-ended voltage measurement. The measured voltage is band-pass filtered with a filter whose center frequency is at the injection frequency f_{inj}, in order to remove any possible measurement noise, as well as any components resulting from harmonics of the injected current. The speed information can then be extracted from the measured voltage by amplitude demodulation as shown in **Fig. 2(b)**. A phase-sensitive rectification, as discussed in detail in [4], can be used for differentiating positive and negative velocities. On the other hand, in applications where the direction of movement is not required, the speed can also be estimated by a simpler, phase-insensitive rectification.

III. Modeling, Design Aspects and Optimization

Models describing the electromagnetic behavior of the considered speed sensor are needed for optimizing the sensor geometry as well as the injection frequency for a given air gap and speed range. Important work on the analytical modeling of a similarly arranged eddy-current-based speed sensor for a moving solid body has been presented in literature. In [3] and [5], the authors discuss the case of circular injection and pick-up coils, whereas a rectangular injection coil of arbitrary orientation towards the conducting plane is modeled in [6] and [7].

However, these works do not consider the use of a magnetic yoke, which shields the sensor from its environment and increases the air gap flux density. Even though it may be computationally more demanding compared to the above-mentioned modeling approaches, finite-element method (FEM) simulations offer an easy-to-set-up and very flexible modeling environment. Therefore, two-dimensional (2-D) time-transient FEM simulations are used for modeling the speed sensor featuring a magnetic yoke.

Key degrees of freedom in the speed sensor design are the geometries of the coils and the yoke, as well as the amplitude and the frequency of the injected current. For a given speed range and air gap, the design goal is to obtain a high sensitivity that results in a voltage range that can be measured using simple signal electronics. A linear sensor characteristic is also desired since it makes the processing easier.

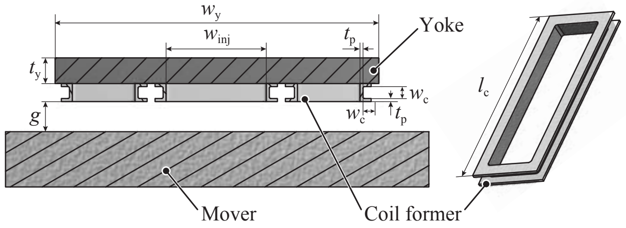

Fig. 3: Cross-sectional view of the speed sensor geometry (left), and the geometry of a 3-D printed coil former (right), with key geometric parameters.

TABLE I: Design Parameters

Symbol	Parameter name	Value
w_y	Yoke width	64 mm
t_p	Plastic wall thickness	0.6 mm
t_y	Yoke thickness	5.1 mm
w_c	Coil side width	2.4 mm
l_c	Coil length	50 mm
g	Air gap (nominal)	8 mm
v	Mover speed	0 .. 12 m/s
a	Mover acceleration	5 m/s^2
	Yoke material	Ferrite N87
	Mover material	Aluminum Ac-112

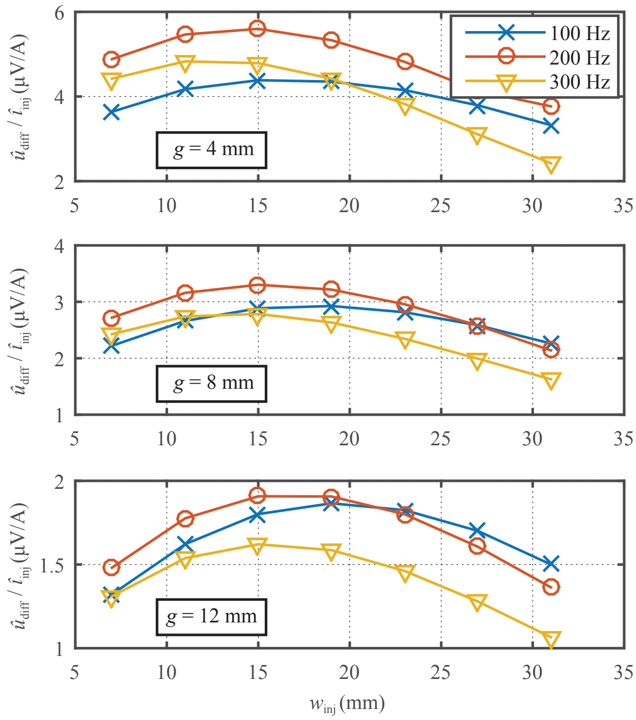

Fig. 4: Simulation results showing the ratio $\hat{u}_{\text{diff}}/\hat{i}_{\text{inj}}$ for air gaps of g = 4 mm (top), 8 mm (middle) and 12 mm (bottom). Three different injection frequencies (f_{inj} = [100 200 300] Hz) are considered. The speed of the mover is v = 12 m/s. It can be seen that the injection coil width of w_{inj} = 15 mm, and the injection frequency of f_{inj} = 200 Hz lead to the highest $\hat{u}_{\text{diff}}/\hat{i}_{\text{inj}}$ (hence, highest sensitivity) for most of the simulated cases.

Neglecting magnetic saturation, the measured voltage u_{diff} (and hence the sensitivity) for a given air gap g and speed v can be increased by increasing the total Ampere-turns of the injected current. Here, possible limits are the energy consumption of the sensor and the heating of the injection coil due to power dissipation.

The relationship between the sensitivity and the injection frequency is more complicated due to the skin effect in the mover, as it will be analyzed in detail later in this paper.

Further design considerations are the overall sensor volume as well as the partitioning of the sensor area between the injection and pick-up coils. The minimization of the sensor size is not a primary goal in this work; therefore, at a first step the sensor area is set by choosing a commercially available, [64 x 50 x 5.1] mm ferrite block as the yoke. The partitioning of the injection and the pick-up coil areas, on the other hand, plays a major role in the performance of a sensor with given volume. Hence, the injection coil width is regarded as a design degree-of-freedom in the optimization, together with the injection frequency. **Fig. 3** shows the key design parameters together with **Tab. I**. Both the injection and pick-up coils are wound using 3-D printed coil formers. For ease of manufacturing, the design is limited to only non-overlapping (i.e. concentrated) coils.

Fig. 4 shows the simulation results for the amplitude of the differential voltage $\hat{u}_{\text{diff}}$ for $\hat{i}_{\text{inj}} = 1$ A and one-turn injection and pick-up coils. The mover speed is $v = 12$ m/s. Air gaps of $g = [4\ ,\ 8,\ 12]$ mm, as well is injection frequencies of $f_{\text{inj}} = [100,\ 200,\ 300]$ Hz are analyzed. It can be seen that, an optimum w_{inj} exists with the maximum sensitivity for each analyzed air gap and injection frequency. For all the analyzed air gaps, $w_{\text{inj}} = 15$ mm, which results in identical injection and pick-up coil geometries, and $f_{\text{inj}} = 200$ Hz leads to the highest sensitivity.

TABLE II: Parameters of the Sensor Prototype

Symbol	Parameter name	Value
w_{inj}	Injection coil width	15 mm
N_{inj}	Injection coil winding turns	70
R_{inj}	Injection coil DC resistance	3.8 Ω
L_{inj}	Injection coil inductance (200 Hz)	485 μH
$N_{\text{pick-up}}$	Pick-up coil turns number	200

IV. Experimental Analysis

Following the initial analysis described above, a speed sensor prototype is built in order to verify the simulations. **Fig. 5** (top) depicts the sensor prototype and **Tab. II** lists its key parameters. The test setup depicted in **Fig. 5** (bottom) is used for the experimental analysis. A drive machine is used to rotate an aluminum wheel, whose surface speed is measured with the speed sensor prototype that is mounted on an adjustable positioning table for an easy variation of the air gap. The encoder at the drive machine's shaft also provides a reference rotational speed measurement.

A digital signal generator and a linear amplifier are used for injecting an AC current with a fixed amplitude into the

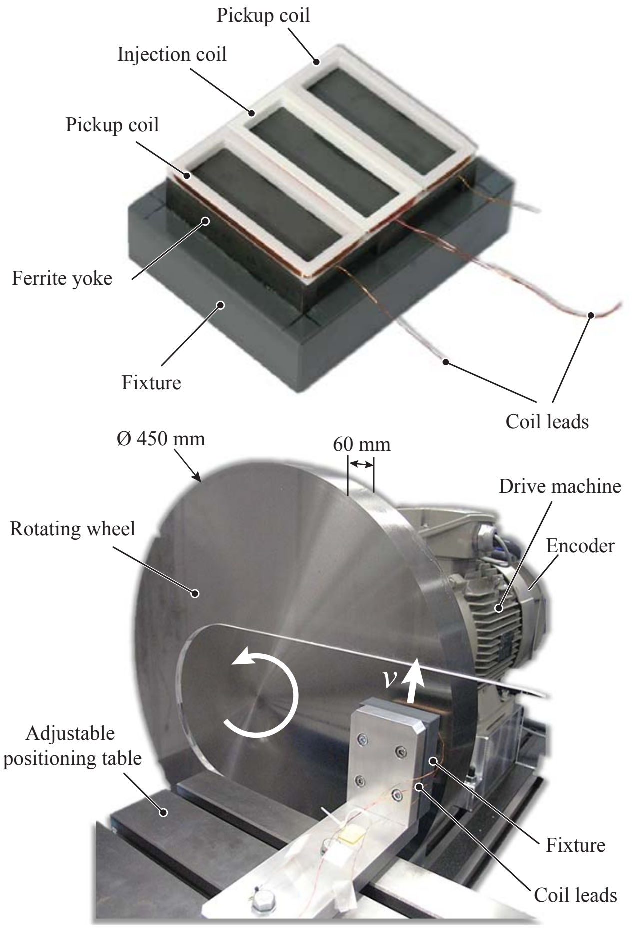

Fig. 5: (Top) Sensor prototype with equally sized injection and pick-up coils ($w_{\text{inj}} = 15$ mm, cf. **Fig. 3**). The 3-D printed coil formers are glued onto the ferrite yoke, which is glued on the fixture. (Bottom) Test bench comprising a drive machine, an aluminum wheel and the speed sensor prototype mounted on an adjustable positioning table. The encoder mounted on the shaft of the drive machine provides reference speed measurements.

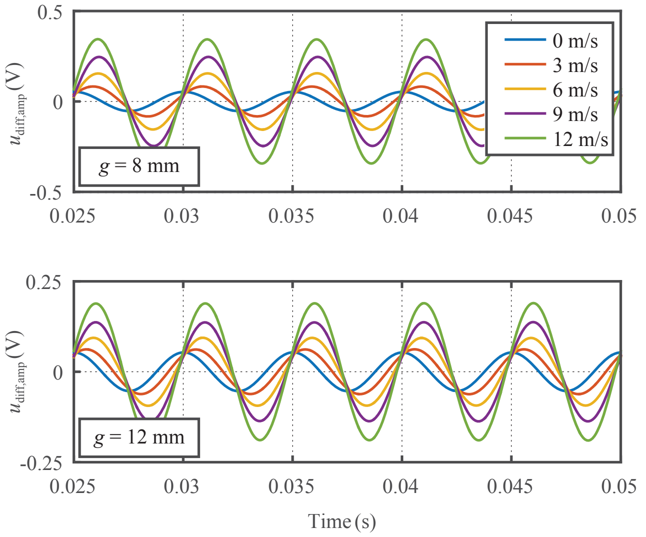

Fig. 6: Measurement results for air gaps of $g = 8$ mm (top), and $g = 12$ mm (bottom). The injection frequency is $f_{\text{inj}} = 200$ Hz, and the injection current amplitude is $\hat{i}_{\text{inj}} = 353$ mA. It can be seen that a non-zero voltage exists for $v = 0$ m/s, as a result of asymmetry due to manufacturing and positioning tolerances.

injection coil. For all the measurements presented in this paper, the amplitude of the current is set to $\hat{i}_{\text{inj}} = 353$ mA ($I_{\text{inj}} = 250$ mA$_{\text{RMS}}$), resulting in a power dissipation of $P_{\text{inj}} = I_{\text{inj}}^2 R_{\text{inj}} = 240$ mW in the injection coil. Since the goal is the verification of the electromagnetic design, the construction of dedicated filtering and amplitude demodulation hardware is omitted at this stage, and a digital oscilloscope is used for measuring the voltage $u_{\text{diff,amp}}$, which is obtained by amplifying the voltage u_{diff} 20 times using a simple operational amplifier circuit in a non-inverting configuration. For having full flexibility, the filtering and demodulation steps are realized as post-processing in a computer, once the voltage waveform is recorded with the oscilloscope. All the measurement results presented in the further sections are band-pass filtered using a 2$^{\text{nd}}$-order Butterworth filter whose lower and upper cut-off frequencies are set to $0.8 f_{\text{inj}}$ and $1.2 f_{\text{inj}}$, respectively.

A. *Offset and Verification of FEM Simulations*

Fig. 6 depicts the measured voltage $u_{\text{diff,amp}}$ for $f_{\text{inj}} = 200$ Hz and $g = [8,\ 12]$ mm. It can be seen that a non-zero voltage exists for $v = 0$ m/s, which will henceforth be called the offset voltage. It results from an unequal flux linkage of the pick-up coils at standstill, and is caused by manufacturing tolerances (i.e. the sensor not being perfectly symmetrical). For a direct comparison of the results with the FEM simulations, where a symmetrical structure is assumed, the offset is removed by an offline, time-domain subtraction from the measured $u_{\text{diff,amp}}$ at non-zero speeds. However, more practical ways of offset removal are also discussed in the following sections.

The comparison of $u_{\text{diff,amp}}$ waveforms calculated by FEM simulations to the measurement results is done in **Fig. 7**, for $f_{\text{inj}} = 200$ Hz and $g = 8$ mm. It can be seen that, the simulations are able to predict both the amplitude's stronger, and the phase's weaker dependencies on the speed accurately.

B. *Sensitivity and Linearity*

Since the amplitude has a higher sensitivity to the speed, the phase change is disregarded at the first step for evaluating the effect of the injection frequency on the sensitivity and linearity of the sensor. **Fig. 8** shows the simulated and measured amplitudes of the measured voltage $u_{\text{diff,amp}}$ for different injection frequencies and air gaps. It can be seen that around $v = 12$ m/s, $f_{\text{inj}} = 100$ Hz is resulting in a strongly non-linear response, showing that the minimum injection frequency should be chosen considering the maximum speed to be measured. It is also seen that an optimum f_{inj} exists, i.e., increasing f_{inj} above 200 Hz leads to a smaller sensitivity,

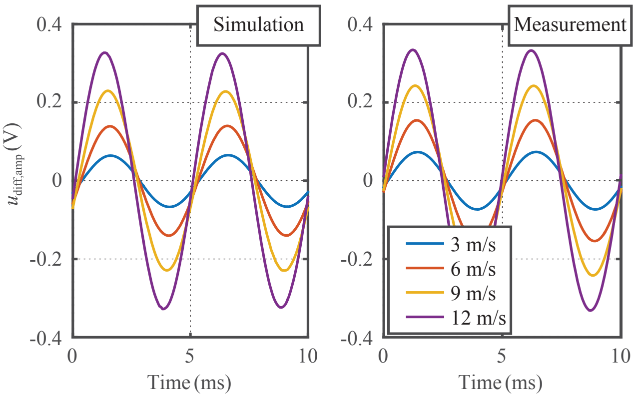

Fig. 7: Simulation (left) and measurement (right) results for an air gap of $g = 8$ mm, injection frequency of $f_{\text{inj}} = 200$ Hz, injection current amplitude of $\hat{i}_{\text{inj}} = 353$ mA. It can be seen that the simulation and measurement results agree very well after the offset is removed from the measurements.

which is attributed to the skin effect in the mover. Finally, it is also noted that the simulations and measurements agree over this wide design range with a total average mismatch below 10%, which is expected to be originating from 3-D (end) effects, as well as the discrepancies between the assumed and actual electrical conductivities of the mover, and between the assumed linear motion and the actual curvature of the aluminum wheel.

C. Effect of the Air Gap

The effect of the air gap g on the measured voltage $u_{\text{diff,amp}}$ can be seen in **Fig. 9**, where measured voltage is plotted, with and without offset correction (by a time-domain subtraction), for different values of f_{inj}, g and v. It can be seen that the air gap plays a significant role in the resulting sensitivity, and the effect of the offset becomes less pronounced at smaller air gaps.

D. Amplitude Demodulation and Dynamic Behavior

Finally, both the removal of the offset through a phase-sensitive demodulation, and the dynamics of the sensor are demonstrated together in **Fig. 10**, where the speed of the mover is changed with $a = \pm 5$ m/s^2. In this case, there is no time-domain subtraction; instead, the band-pass filtered signal is demodulated by a multiplication with a clock signal in the form of $u_{\text{clk}} = \text{sign}(i_{\text{inj}})$. Even though this is done offline in software, a real-time hardware realization would be possible with a zero-crossing detector and simple signal electronics [4]. The demodulated signal is low-pass filtered with a 2$^{\text{nd}}$-order Butterworth filter whose cut-off frequency is set to 20 Hz, and a gain of 57 m/Vs is applied to obtain the speed as plotted in **Fig. 10**.

V. Conclusion

Measuring the angular or translational velocity of a solid body in motion is crucial for the monitoring and/or control of numerous industrial processes. A direct mechanical contact of the speed sensor to the mover is either undesired or strictly prohibited, e.g. due to wear and reliability concerns. Several contactless speed sensors are widely used today, such as magnetic or optical devices. However, these devices are either not well-suited for operation in harsh environments (e.g. optical sensors are susceptible to dirt), or they require a spatial variation of the physical quantity that they measure, and cannot be used for measuring the speed of smooth surfaces (e.g. variable reluctance sensors rely on the spatial variation of a magnetic air gap). Therefore, a contactless speed sensor that is well-suited for estimating the speed of an electrically conductive, smooth surface is developed in this work.

The analyzed speed sensor comprises an injection coil, which induces eddy currents in the mover. At standstill, the eddy-current distribution is symmetrical, but it gets skewed with increasing speeds. The reaction field is detected via two differentially wound pick-up coils placed on both sides of the injection coil. Signal conditioning steps of filtering and amplitude demodulation are used for extracting the speed information from the difference of the voltages induced in the pick-up coils.

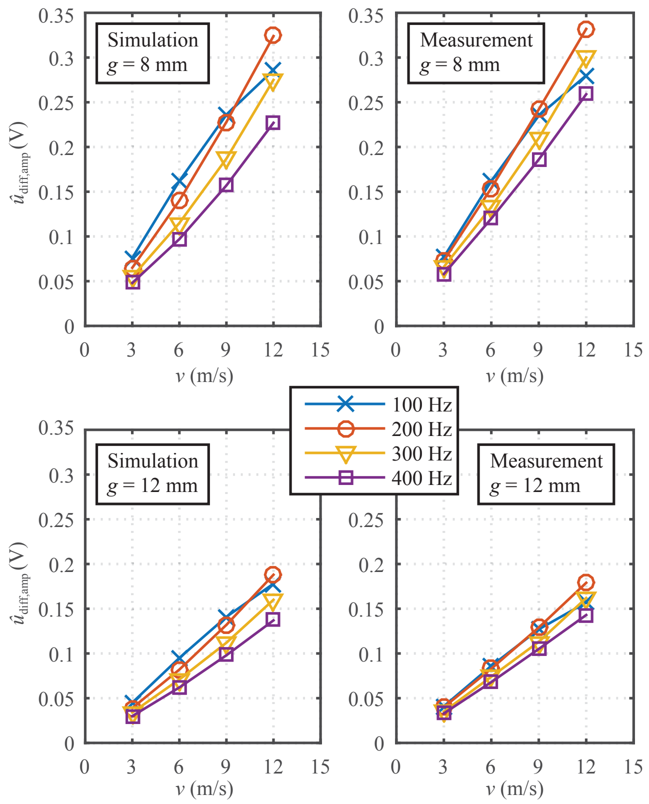

Fig. 8: Simulation (left) and measurement (right) results for air gaps of $g = 8$ mm (top) and $g = 12$ mm (bottom). Injected current amplitude is $\hat{i}_{\text{inj}} = 353$ mA. It can be seen that the simulation and measurement results agree very well, with an average mismatch below 10% for $g = 8$ mm and below 6% for $g = 12$ mm.

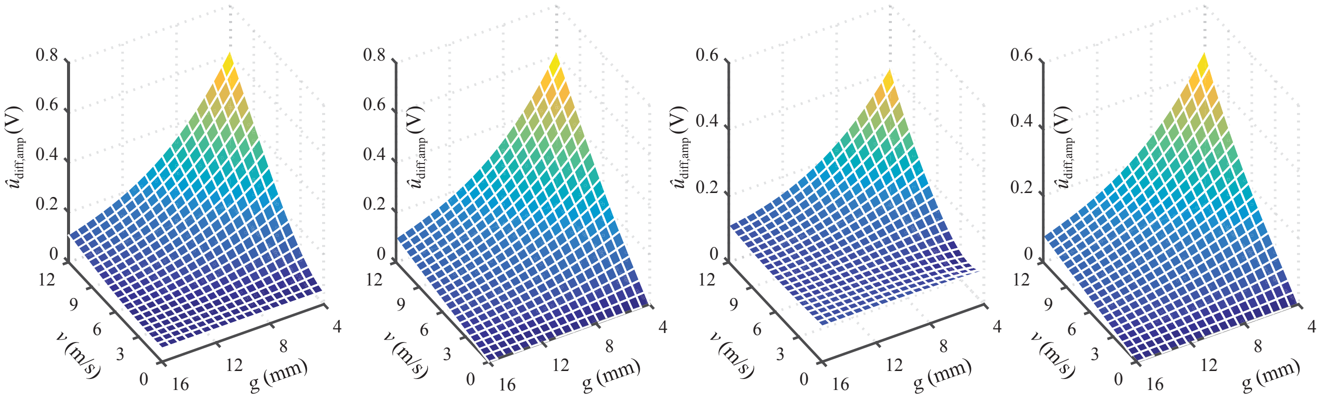

(a) (b) (c) (d)

Fig. 9: Measurement results showing $u_{\mathrm{diff,amp}}$ for different mover speeds and air gaps, for f_{inj} = 200 Hz ((a) and (b)), f_{inj} = 400 Hz ((c) and (d)). The amplitudes are plotted as measured in (a) and (c); whereas, the offset is corrected by a time-domain subtraction in (b) and (d).

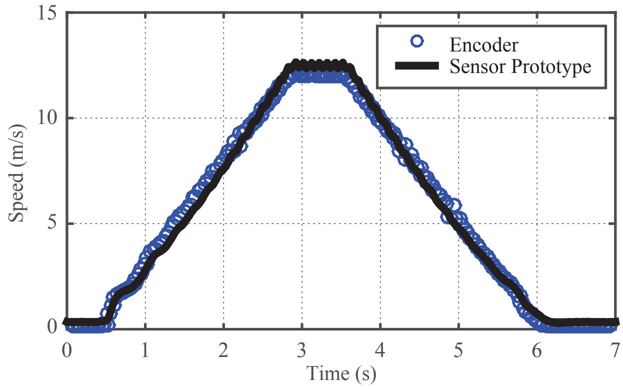

Fig. 10: Mover speed, as recorded by the encoder and the speed sensor prototype. The encoder reading is converted to surface speed as $v = \omega r$ where ω is the mechanical angular velocity and $r = 192$ mm. The low-pass filtered output voltage of the eddy-current-based speed sensor is converted to speed by multiplication with the constant 57 m/Vs. The air gap is $g = 8$ mm, and the injection frequency is f_{inj}= 200 Hz.

The models presented in literature are enhanced by including a magnetic yoke, which shields the sensor and amplifies the sensitivity for a given power consumption by intensifying the air gap flux. The outer volume of the sensor is fixed in this work, but the optimal partitioning of the injection and pick-up coil areas as well as the optimum injection frequency are studied.

A prototype is built and the design procedure is verified experimentally. It is found that the voltages induced in the two pick-up coils are not identical at standstill, as a result of small asymmetries in the construction due to manufacturing tolerances. However, a simple phase-sensitive demodulation approach is shown to alleviate the effect of this offset voltage on the sensor performance.

The future work will focus on the design and construction of dedicated hardware for the implementation of filtering and demodulation steps, as well as signal injection. Also the trade-off between the sensor volume and sensitivity will be investigated for various air gaps, and movers made of different materials.

Acknowledgment

The authors would like to express their sincere appreciation to Nabtesco Corp., Japan, for the financial and technical support of research on energy harvesting technologies at the Power Electronic Systems Laboratory, ETH Zurich, which provided the basis for achieving the results presented in this paper. In particular, inspiring technical discussions with K. Nakamura, Y. Tsukada and Y. Ono are acknowledged. Moreover, the authors acknowledge the support of CADFEM (Suisse) AG concerning the ANSYS software.

References

[1] J. M. Lopera, M. J. Prieto, F. F. Linera, G. Vecino, and J. A. Gonzlez, "A new speed measurement system," *IEEE Industry Applications Magazine*, pp. 44–51, November/December 2005.

[2] S. Hensel, T. Strau, and M. Marinov, "Eddy current sensor based velocity and distance estimation in rail vehicles," *IET Science, Measurement Technology*, vol. 9, no. 7, pp. 875–881, 2015.

[3] N. Takehira, A. Tanaka, and K. Toda, "Analysis of a speed meter utilizing eddy current effect," *Electrical Engineering in Japan*, vol. 97, no. 5, pp. 1–8, September 1977, translated from *Denki Gakkai Ronbunshi*, vol. 97A, no. 9, pp. 457-464, September 1977.

[4] A. Tüysüz and J. W. Kolar, "New position-sensing concept for miniature lateral-stator machines," *IEEE Transactions on Industrial Electronics*, vol. 63, no. 6, pp. 3489–3498, June 2016.

[5] N. Takehira and A. Tanaka, "Analysis of transmission type speedometer utilizing eddy current effect," *Electrical Engineering in Japan*, vol. 100, no. 5, pp. 1–7, September 1980, translated from *Denki Gakkai Ronbunshi*, vol. 100A, no. 9, pp. 483-490, September 1980.

[6] A. Tanaka, N. Takehira, and K. Toda, "Analysis of a rectangular coil facing a moving sheet conductor," *Electrical Engineering in Japan*, vol. 101, no. 4, pp. 15–22, August 1981, translated from *Denki Gakkai Ronbunshi*, vol. 101A, no. 8, pp. 405-412, August 1981.

[7] A. Tanaka and N. Takehira, "Eddy current speed meter using galvano-magnetic devices," *Electrical Engineering in Japan*, vol. 106, no. 4, pp. 29–36, June 1986, translated from *Denki Gakkai Ronbunshi*, vol. 106A, no. 4, pp. 267-274, June 1986.